A Reexamination of Active and Passive Tumor Targeting by Using Rod-Shaped Gold Nanocrystals and Covalently Conjugated Peptide Ligands

Xiaohua Huang,[†,‡,∥] Xianghong Peng,[§,∥] Yiqing Wang,[†] Yuxiang Wang,[§] Dong M. Shin,[§,*] Mostafa A. El-Sayed,[⊥,*] and Shuming Nie[†,*]

[†]Departments of Biomedical Engineering and Chemistry, Emory University and Georgia Institute of Technology, 101 Woodruff Circle Suite 2007, Atlanta, Georgia 30322, United States, [‡]Department of Chemistry, The University of Memphis, 411 Smith Chemistry Building, Memphis, Tennessee 38152, United States, [§]Department of Hematology and Medical Oncology and the Winship Cancer Institute, Emory University, School of Medicine, 1365 Clifton Road, Atlanta, Georgia 30322, United States, and [⊥]Laser Dynamics Laboratory, School of Chemistry and Biochemistry, Georgia Institute of Technology, Atlanta, Georgia 30332, United States. [∥]Authors contributed equally to this work.

ABSTRACT The targeted delivery of nanoparticles to solid tumors is one of the most important and challenging problems in cancer nanomedicine, but the detailed delivery mechanisms and design principles are still not well understood. Here we report quantitative tumor uptake studies for a class of elongated gold nanocrystals (called nanorods) that are covalently conjugated to tumor-targeting peptides. A major advantage in using gold as a "tracer" is that the accumulated gold in tumors and other organs can be quantitatively determined by elemental mass spectrometry (gold is not a natural element found in animals). Thus, colloidal gold nanorods are stabilized with a layer of polyethylene glycols (PEGs) and are conjugated to three different ligands: (i) a single-chain variable fragment (ScFv) peptide that recognizes the epidermal growth factor receptor (EGFR); (ii) an amino terminal fragment (ATF) peptide that recognizes the urokinase plasminogen activator receptor (uPAR); and (iii) a cyclic RGD peptide that recognizes the $\alpha_v\beta_3$ integrin receptor. Quantitative pharmacokinetic and biodistribution data show that these targeting ligands only marginally improve the total gold accumulation in xenograft tumor models in comparison with nontargeted controls, but their use could greatly alter the intracellular and extracellular nanoparticle distributions. When the gold nanorods are administered via intravenous injection, we also find that active molecular targeting of the tumor microenvironments (*e.g.*, fibroblasts, macrophages, and vasculatures) does not significantly influence the tumor nanoparticle uptake. These results suggest that for photothermal cancer therapy, the preferred route of gold nanorod administration is intratumoral injection instead of intravenous injection.

KEYWORDS: tumor targeting · nanoparticle delivery · gold nanorod · peptide · lung cancer · EGFR · uPAR · RGD

The targeted delivery of nanoparticles to solid tumors is a key task in the development of cancer nanomedicine for *in vivo* molecular imaging and targeted therapy.[1−8] Despite extensive research and significant progress in the last 10−15 years, there are still major fundamental and technical barriers that need to be understood and overcome.[1−9] These problems include the complex interactions between naoparticles and biological systems *in vivo*, rapid uptake and clearance of nanoparticles by the reticuloendothelial system (RES) organs (such as the liver and spleen), and very limited penetration of nanoparticles to poorly vascularized or necrotic tumor regions.[2,10] Current methods for nanoparticle delivery are mainly based on an "active" mechanism and a "passive" mechanism.[9,10] In the active mode, molecular ligands such as antibodies, peptides, or small molecules are used to recognize specific receptors on the tumor cell surface, often followed by receptor-mediated endocytosis and nanoparticle internalization. In the passive mode, nanoparticles without targeting ligands are accumulated and retained in the tumor interstitial space mainly through the enhanced permeability and retention (EPR) effect.[11−13] In both mechanisms, a common feature is that nanoparticles in the bloodstream must first move across the tumor blood vessels (usually leaky vasculatures) and extravasate into the tumor interstitium or the perivascular region.[11]

Under this general framework, however, there is still considerable debate about the relative contributions of such active and passive targeting mechanisms.[14] Recent work by several groups has shown that the use of tumor-targeting ligands does not increase the total accumulation of nanoparticles in solid tumors, although it does function to increase receptor-mediated internalization and could thus improve therapeutic efficacy for cancer drugs that act on intracellular protein targets.[14−17] In particular, Park and co-workers[15] have

*Address correspondence to dmshin@emory.edu; melsayed@gatech.edu; snie@emory.edu

Received for review August 16, 2010 and accepted September 17, 2010.

Published online September 23, 2010.
10.1021/nn102055s

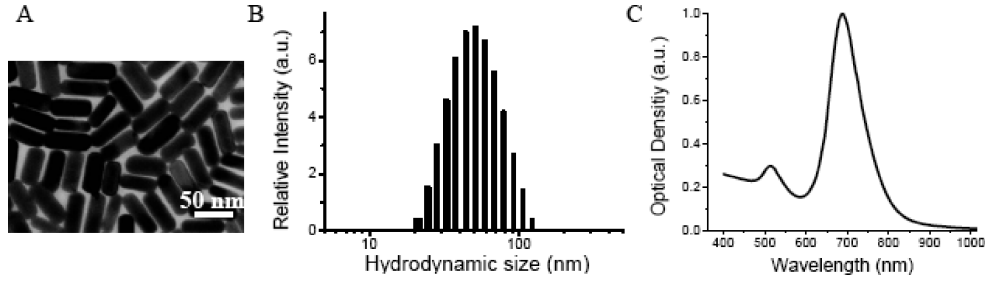

Figure 1. Structure and optical properties of as-synthesized Au NRs: (A) TEM micrograph showing that the NRs have an aspect ratio of 3; (B) dynamic light scattering data showing an average hydrodynamic size of 51 nm; and (C) optical absorption spectrum showing two surface plasmon resonance peaks at 520 and 680 nm.

shown that PEGylated liposomes linked with anti-HER2 antibodies are internalized into tumor cells, but their total tumor accumulation is not different from that of nontargeted particles. Davis and co-workers[16,17] have also reported that transferrin targeting improves the intracellular localization of polymeric nanoparticles, but does not increase their total tumor uptake. In addition, theoretical modeling studies by Wittrup and co-workers[18] reveal that the total tumor uptake of liposomes is not enhanced by conjugation to targeting ligands.

There is also a considerable amount of opposing data showing that the use of tumor-targeting ligands is effective in delivering imaging and therapeutic agents into solid tumors.[19−24] For example, tumor-targeting studies using fluorescently and radioactively labeled antibodies have shown higher tumor uptake (measured on the basis of per gram of tumor mass) for macromolecules and nanoparticles than their nontargeted controls.[25,26] Complicating this matter further, recent work has shown that that the use of targeting ligands might even be "detrimental" because the exposed ligands can accelerate nanoparticle opsonization (adsorption of blood proteins) and blood clearance, leading to an overall reduction in tumor nanoparticle uptake.[27−29] Regarding the effects of nanoparticle structure and shape, Discher, Sailor, and their co-workers[30,31] have shown that elongated nanoparticles (called nanofilaments and nanoworms) have longer blood circulation times and show improved accumulation in solid tumors in comparison with their spherical counterparts.

Here we report quantitative tumor uptake studies for elongated gold nanocrystals (called nanorods, NRs) that are covalently conjugated to targeting peptide ligands. A major advantage in using gold (Au) as a "tracer" is that the amount of accumulated Au can be quantitatively determined by inductively coupled plasmon−mass spectrometry (ICP-MS), a common procedure for elemental analysis.[32] Also, Au NRs have novel optical and electronic properties and have broad applications in cellular imaging,[33−39] biosensing,[40−42] surface-enhanced Raman scattering (SERS),[43,44] and near-infrared photothermal therapy.[33,45−49] By using animal models bearing A549 lung tumors, we have examined the pharmacokinetic and biodistribution properties of both targeted and nontargeted Au nanocrystals. The A549 xenograft tumors are especially well suited for nanoparticle targeting studies because of their high expressions of several extracellular receptors including the epidermal growth factor receptor (EGFR), the urokinase plasminogen activator receptor (uPAR), and the $a_v\beta_3$ integrin receptor.[50−54] Thus, we have used a single-chain variable fragment peptide (ScFv, 25 KD, K_d = 3.4 nM) to target EGFR, an amino-terminal fragment peptide (ATF, 15 KD, K_d = 0.1 nM) to target uPAR, and a cyclic RGD peptide (0.9 KD, K_d = 2 nM) to target the $a_v\beta_3$ receptor.

It is worth noting that the uPAR and $a_v\beta_3$ receptors are broadly expressed in the tumor stroma and/or on the surface of tumor blood vessels,[55−57] so the use of ATF and RGD ligands could allow active targeting of both the tumor cells and the tumor microenvironments. In fact, we had hypothesized targeting tumor stroma and vasculatures could be more effective than targeting tumor cells because the circulating nanoparticles are expected to encounter the tumor vasculature and stroma before binding to tumor cells. However, our quantitative ICP-MS data show that active targeting of tumor cells or the tumor microenvironments only marginally improves the total tumor uptake of gold nanoparticles. The main differences caused by active targeting are observed in the distribution patterns of nanoparticles inside tumor cells and in the tumor microenvironments. These results suggest that nano-

TABLE 1. Properties of As-Synthesized, PEG-Coated, and Peptide-Conjugated Gold Nanorods[a]

surface ligands	hydrodynamic diameter (nm)	zeta potential (mV)
CTAB	51 ± 2	+40 ± 5
mPEG-SH 5k	68 ± 2	−5 ± 3
mPEG-SH 5k/HS-PEG-COOH 5k	78 ± 3	−25 ± 2
ScFv EGFR	79 ± 3	−15 ± 2
ATF	80 ± 3	−19 ± 2
c-RGD	81 ± 2	−16 ± 2

[a]Abbreviations: CTAB = cetyltrimethylammonium bromide; mPEG-SH = thiolated methoxy-poly(ethylene) glycol; HS-PEG-COOH = thiolated carboxy-poly(ethylene) glycol; ScFv EGFR = single-chain variable fragment of anti-epidermal growth factor receptor; ATF = amino-terminal fragment of urokinase plasminogen activator; c-RGD = cyclic arginine-glycine-aspartate.

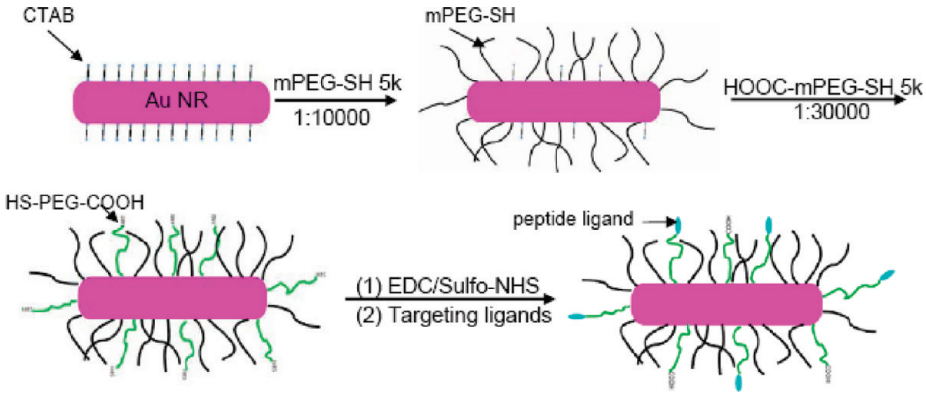

Figure 2. Stabilization and bioconjugation of Au NRs for cellular and *in vivo* tumor targeting. Surfactant-capped nanorods are first stabilizied by using methoxy-PEG-SH, followed by carboxy-PEG-SH. The functional carboxy (−COOH) groups are activatetd by using EDC/Sulfo-NHS and are covalently conjugated to tumor-targeting peptides via stable amide bonds. Approximately 400−500 peptide molecules are conjugated to each Au NR. See text for discussion.

particle delivery is likely limited by mass transport across the tumor vasculature, at least for large and rigid nanoparticles such as Au NRs. Thus, for photothermal cancer therapy using large nanorods, the preferred route of administration is direct tumor injection, not intravenous systemic injection.

RESULTS AND DISCUSSION

Properties of Au NRs and Ligand Conjugation. Au NRs were synthesized according to the seed-mediated growth method of Nikoobakht and El-Sayed.[58] The "as-synthesized" Au NRs have an aspect ratio (length-to-width) of 3.0, an average hydrodynamic size (diameter,

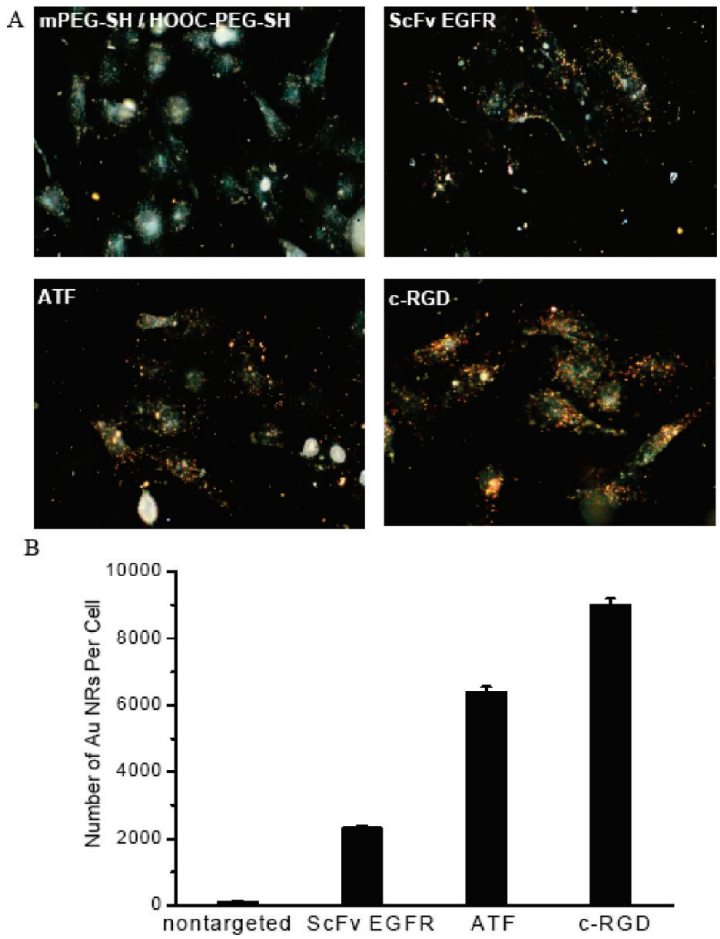

Figure 3. (A) Dark-field imaging and (B) quantitative Au ICP-MS studies of NR binding to cultured A549 cancer cells. The data show specific binding of peptide-conjugated Au NRs to cultured A549 lung cancer cells, and negligible binding of nontargeted particles to the same tumor cells. Cells were incubated with 1 nM Au NRs for 2 h at 37 °C in the culture medium and were washed with 1× PBS buffer. After trypsin treatment, approximately one million cells were counted and analyzed to minimize statistical errors.

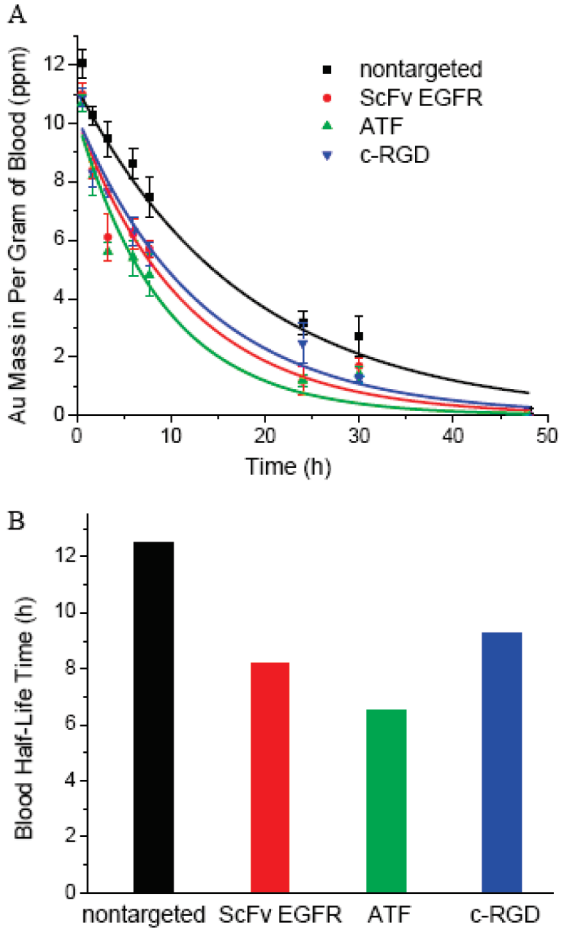

Figure 4. Blood circulation and pharmacokinetic data obtained for targeted and nontargeted Au NRs in healthy mice models. Au NRs were injected via tail veins, and their blood concentrations were measured by ICP-MS analysis of blood samples at various time intervals (0 to 48 h). The measured blood halftime ($t_{1/2}$) is 12.5 h for the control particles, 8.5 h for the ScFv EGFR particles, 6.5 h for the ATF particles, and 9.3 h for the c-RGD particles.

or *D*) of 51 nm, a positive surface charge (zeta potential, or ζ) of 40 mV, and two prominent surface plasmon resonance (SPR) peaks located at 520 and 680 nm (see Figure 1 and Table 1). Note that a cationic surfactant (cetyltrimethylammonium bromide, or CTAB) is used to cap and stabilize the nanorods during synthesis, and this surfactant forms a bilayer structure on the nanorod surface, giving rise to the positive surface charge measured by dynamic light scattering (DLS). For colloidal stability, biocompatibility, and ligand conjugation, the Au NRs are coated with a mixed layer of two thiolated PEGs (methoxy-PEG, or mPEG, and carboxy-PEG, or HOOC-PEG, both 5000 MW) in two separate steps. As illustrated in Figure 2, the NRs are first stabilized by using mPEG-SH (neutral) and then by HOOC-PEG-SH in a sequential manner. This process introduces functional −COOH groups for peptide conjugation, and the sequential procedure is necessary to avoid nanoparticle aggregation, a major problem when CTAB-capped NRs (positively charged) are exposed directly to HOOC-PEGs (negatively charged). Dynamic light scattering data reveal that the first mPEG coating step increases the particle hydrodynamic size by 18 nm and decreases the surface potential by 33 mV. The HOOC-PEG coating step further increases the hydrodynamic size by 10 nm and decreases the zeta potential by 20 mV.

To determine the number of attached PEG molecules on each nanorod, we have used an amine-terminated PEG (NH_2-PEG-SH, MW 5000) to replace mPEG or HOOC-PEG for NR coating. The number of primary amine groups is determined by using *N*-succinimidyl 3-(2-pyridyldithio)propionate (SPDP), a colorimetric agent that generates pyridine-2-thione and can be quantified by UV−vis absorption.[59] The results indicate that each Au NR is coated with approximately 7500 mPEG molecules and 4300 HOOC-PEG molecules. We note that these numbers are only rough estimates because we have not quantitatively determined the reproducibility and accuracy of the indirect colorimetric procedure. To avoid this uncertainty, we have used the same batch of pegylated gold nanorods for both control studies and for conjugation to the various targeting ligands. So, the control and targeted nanorods should have the same amounts of mPEG and HOOC-PEG. The final PEG-protected NRs are stable even under high-salt and strong acid/base conditions, allowing covalent conjugation to peptide ligands via amide bonds by using EDC/sulfo-NHS coupling reactions. Under our experimental conditions, the overall peptide conjugation efficiency is about 40−50%,[60] so starting with 1000 peptide molecules per rod in the reaction mixture, one can expect that each NR is conjugated to 400−500 peptide molecules, a value that is further confirmed by direct protein assays (Bio-Rad protein assay using Coomassie Blue G-250 dyes). Dynamic light scattering data further reveal that this level of ligand conjugation only slightly changes the particle's hydrodynamic size (an increase of 1−3 nm), but reduces the particle's surface charge by as much as 6−10 mV (see Table 1). This is most likely caused by a decrease in free COOH groups after covalent conjugation and by positive charges on the peptide ligands.

Cellular Binding and Uptake. As mentioned earlier, the A549 tumor is used as an animal model for aggressive and metastatic non-small-cell lung carcinoma. Histological staining studies have shown that the xenograft tumors have high expressions of EGFR, uPAR, and $a_v\beta_3$ receptors.[50−54] By using cultured cancer cells, we have obtained *in vitro* cellular binding and uptake data for both targeted and nontargeted Au NRs. As shown in Figure 3, both dark-field imaging and quantitative ICP-MS data demonstrate specific cellular binding of the peptide-conjugated particles that is 20−100 times stronger than the control particles under the same experimental conditions. The amount of bound nanoparticles is believed to depend on the receptor expression level and the ligand−receptor binding affinity, but other factors such as steric hindrance (accessibility)

and the rate of receptor-mediated endocytosis are likely important as well. Taken together, these cellular binding data indicate that (i) the covalent conjugation chemistry is successful; (ii) the conjugated ligands are still able to recognize their target receptors; and (iii) the A549 cancer cells indeed have high expressions of the three extracellular receptors.

Pharmacokinetics. To examine the pharmacokinetic properties of the Au NRs, we have used ICP-MS to measure the Au concentration in blood samples at various time points after tail vein injection (between 0 and 48 h) (see Figure 4). The experimental data can be fitted to a monoexponential decay model, resulting in a half-decay time ($t_{1/2}$) of 12.5 h for the nontargeted nanoparticle (which are coated with a mixture of mPEG and HOOC-PEG), a halftime of 8.3 h for the ScFv-conjugated nanoparticle, a halftime of 6.5 h for the ATF-conjugated nanoparticle, and a halftime of 9.3 h for the cRGD-conjugated nanoparticle. These quantitative data indicate that the addition of tumor-targeting ligands can indeed accelerate nanoparticle opsonization and blood clearance. Previously, Montet et al. reported that the attachment of just 20 c-RGD molecules to each amino-dextran-coated iron oxide nanoparticle reduced the blood circulation halftime by 5 h.[28] Also, McNeeley et al. showed that adding just 0.15% folate to PEGylated liposomes reduced the $t_{1/2}$ value from 18 h to 6.7 h.[29] Clearly, the density of targeting ligands needs to be optimized so that the targeted nanoparticles have sufficiently long blood circulation times for active receptor binding and tumor accumulation.[61]

Tumor and Organ Uptake. Next, we investigated the organ distribution and tumor uptake for both the targeted and nontargeted nanoparticles at 24 h postinjection, again by using ICP-MS to measure the accumulated Au in dried tissues (see Figure 5). As expected, all the Au particles are efficiently taken up by the RES organs (*e.g.*, the liver and spleen), with little accumulation in the kidney or lung. Interestingly, the three peptide-conjugated nanoparticles are taken up more efficiently by the RES organs than the control particle (which has the lowest Au concentration in the liver and spleen). This is perhaps not surprising because the nanoparticles with exposed peptide ligands are less "stealthy" and can be recognized by the immune system for clearance. Also, the ScFv- and ATF-conjugated particles are more efficient in tumor accumulation than the control particle, but the cRGD-conjugated particles show 2−3-fold lower tumor accumulation than the control particles. Considering their similar blood circulation times,

We believe that the low tumor accumulation of the RGD particle is related to its high uptake in the liver and spleen. Kinetic studies have shown that targeted nanoparticles are taken up by tumors faster than nontargeted particles in the short term (within 6 h), but after 20 h, the nontargeted particles often attain a higher

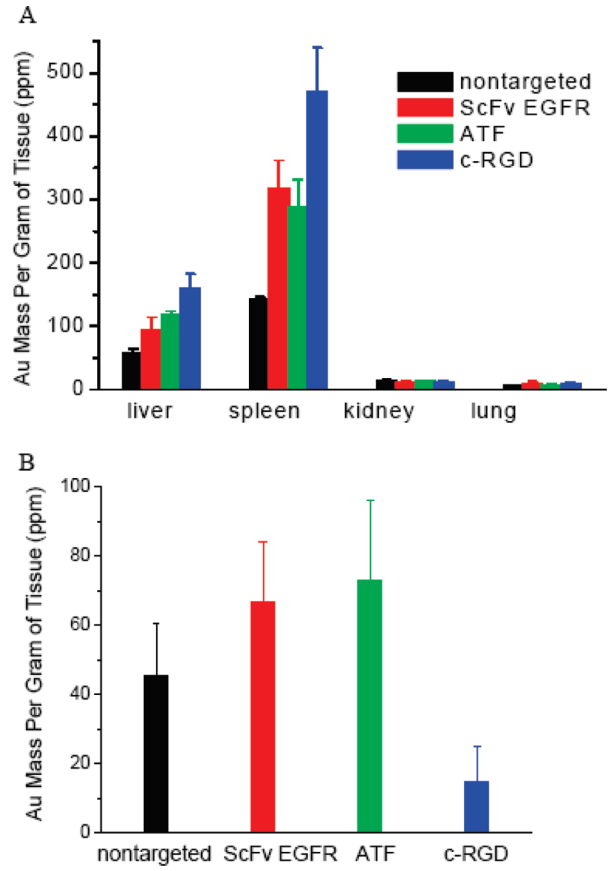

Figure 5. Quantitative organ (A) and tumor (B) uptake data obtained from nontargeted and targeted Au NR conjugates measured by ICP-MS at 24 h postinjection in A549 xenografted mice models. The nontargeted Au NRs showed similar tumor uptake to EGFR- and uPAR-targeted, but 3 times higher than $\alpha_v\beta_3$ integrin-targeted Au NRs.

accumulation level than the targeted particles.[27] To further explore the effect of ligand density on tumor uptake, we have obtained quantitative organ and tumor biodistribution data for nontargeted (control) and cRGD-conjugated Au nanorods at different ligand densities (0, 50, 500, or 5000 cRGD molecules per nanorod) (see Supporting Figure S1). The results indicate that the liver and spleen uptake is increased at higher ligand densities, but the gold accumulation in tumors is significantly reduced for all the ligand densities studied in this work. More data points are still needed to examine the pharmacokinetic and tumor uptake behaviors of targeted gold nanorods at ultralow ligand densities in the range of 1−10 ligand molecules per particle. Also, when the organ and tumor uptake data are analyzed as percentages of injection dose, it becomes clear that the liver and spleen take up 40% of the control nanorods and 60−90% of the targeted nanorods (see Supporting Figure S2). In comparison, the tumors take up only 1−2% of the injected gold nanorods (see Supporting Figure S3). These results indicate that the use of active targeting ligands does not greatly improve the total tumor uptake of nanoparticles, but as discussed

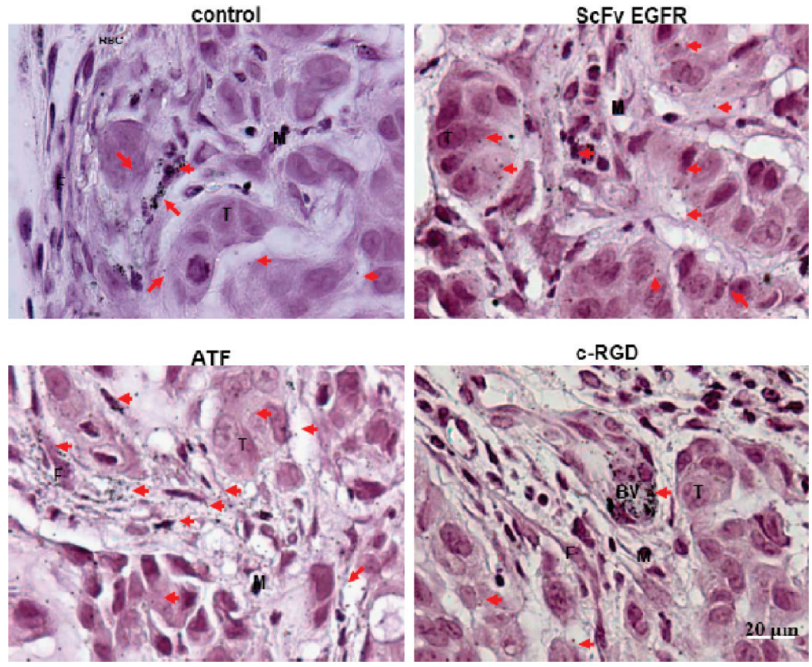

Figure 6. Light microscopic images of silver-enhanced and hematoxylin-stained tumor tissue sections showing intratumoral distribution of targeted and nontargeted Au NRs. Nontargeted Au NRs were mainly randomly distributed in the extracellular matrix but not inside the tumor cells. The ScFv EGFR/Au NRs were mainly located in the cytoplasm of tumor cells, and few particles could be found in the stroma. The ATF/Au NRs were mainly distributed in the stroma, and few particles were internalized by the tumor cells. Most of the RGD/Au NRs are located in the endothelial cells of the blood vessel but not inside the tumor cells. Silver-enhanced Au NRs are marked by arrows; tumor cells by T; macrophage cells by M; fibroblast cells by F; red blood cells by RBC; and blood vessels by BV.

below, the nature of targeting ligands can dramatically change the nanoparticle distribution in the tumor cells and in the tumor microenvironments.

Intratumoral Nanoparticle Distribution. We further examined the intratumoral distributions of targeted and nontargeted Au NRs by using both optical microscopy (via silver enhancement) and transmission electron microscopy (TEM). Silver enhancement renders Au NRs in tissue sections directly visible for observation under bright-field light microscopy. As shown in Figure 6, silver enhancement and hematoxylin staining reveal that the nontargeted Au NRs are mainly localized around blood vessels, in the tumor stromal matrix, and inside some macrophage cells. In contrast, the EGFR-targeted NRs are mainly found inside tumor cells, the uPAR-targeted NRs are predominantly localized in tumor stro-

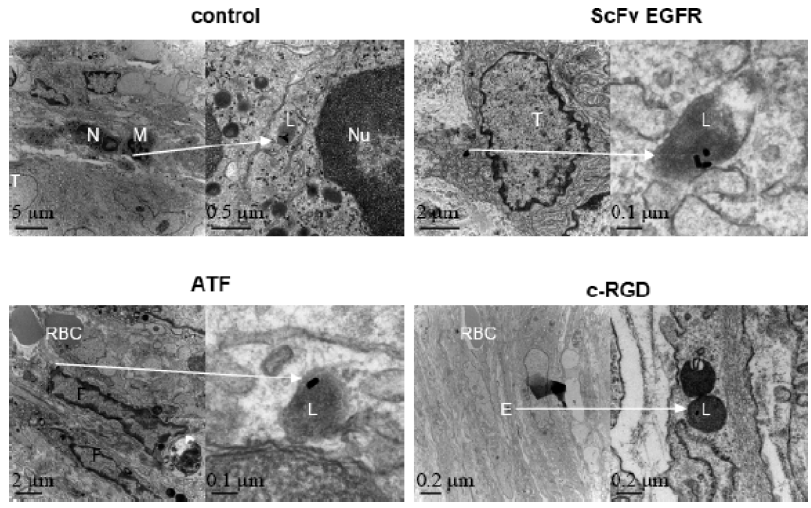

Figure 7. TEM images of tumor tissue sections showing intracellular localization of Au NRs. For each ligand, Au NRs in selected areas (indicated by arrows) are shown in zoomed-in images. The nontargeted NRs were found in the lysosomes of macrophages. ScFv EGFR/Au NRs were located in the endososomes of tumor cells. ATF/Au NRs were found in the endososomes of fibroblasts, and the RGD/Au NRs were mainly distributed in the endososomes of blood vessel endothelial cells. Tumor cells are marked by T; neutrophil cells by N; macrophage cells by M; red blood cells by RBC; vessel endothelial cell by E; cell nuclei by N; and lysosomes by L.

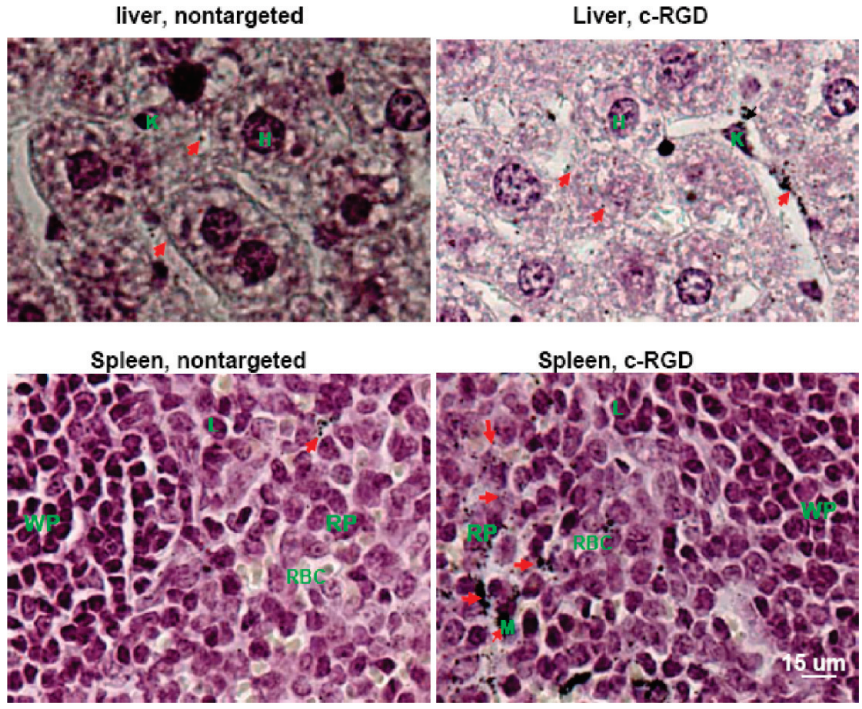

Figure 8. Light microscopic images of silver-enhanced and hematoxylin-stained liver and spleen tissue sections showing intratumoral distribution of nontargeted and $\alpha_v\beta_3$ integrin-targeted Au NRs. In comparison with nontargeted Au NRs, the $\alpha_v\beta_3$ integrin-targeted Au NRs were mainly found in macrophages in the liver and in red pulp region of the spleen with significant higher affinities. Silver-enhanced Au NRs are marked by arrows; hepatocyte cells by H; lymphocyte cells by L; Kupffer cells by K; microphage cells by M; spleen red pulp by RP; and spleen white pulp by WP.

mal cells (but not inside tumor cells), and the integrin-targeted nanorods are accumulated around tumor blood vessels (perivascular regions). These findings are further supported by TEM results (see Figure 7), which show that nanoparticle internalization into tumor cells, fibroblast cells, and endothelial cells is enhanced by using targeting ligands. In particular, the ATF ligand favorably binds to stromal cells, and the c-RGD ligand to blood vessels.

Since Au NRs were mainly accumulated in the RES, we further examined their distribution in the liver and spleen for nontargeted and targeted Au NRs with c-RGD peptide, which is chosen because of their higher uptake than other ligands (see Figure 8). In the liver, targeted Au NRs were found in Kupffer cells or in the Disse space around hepatocytes. Note that the Disse space is located in the liver between hepatocytes and hepatic sinus, and it largely exists in pore structures in the endothelial cells that do not have basement membranes. Thus, the circulating NRs could enter the Disse space and *vice versa*, while the nontargeted ones in the Disse space may diffuse back to the hepatic sinus due to lack of cell uptake. A much lower number of nontargeted particles was found in the Disse region. In the spleen, the targeted NRs were mainly found in red pulp and along sinuses, while the nontargeted particles were much less found along the sinuses.

In summary, we have reported quantitative tumor uptake studies for elongated gold nanocrystals that are covalently conjugated to tumor-targeting peptides. Quantitative pharmacokinetic and biodistribution data from xenograft animal models show that the use of active targeting ligands only marginally improves the total tumor uptake in comparison with control particles. However, the nature of targeting ligands can greatly affect the nanoparticle distribution in the tumor cells and the tumor microenvironments. A surprise finding is that active molecular targeting of the tumor microenvironments (including fibroblasts, macrophages, and vasculatures) does not significantly improve the total tumor accumulation of nanoparticles, at least for long-circulating and rigid gold nanoparticles. These results suggest that mass transport across the tumor vasculature is a rate-limiting step for nanoparticle delivery, and the kinetics of this step is largely unaffected by receptor binding. Thus, for photothermal cancer therapy, the preferred route of gold nanorods is intratumoral administration rather than intravenous injection.

MATERIALS AND METHODS

Synthesis and Characterization of Au NRs. Au NRs were synthesized according to the well-established seed-mediated growth method.[57] In a typical procedure, 600 μL of ice-cold 10 mM sodium borohydride (Sigma-Aldrich, St. Louis, MO, USA) was quickly added to 10 mL of 0.5 mM auric acid ($HAuCl_4$) (Sigma-Aldrich) dissolved in 0.2 M CTAB (Sigma-Aldrich) surfactant solution. The mixture was stirred for 4 min, producing a brown solu-

tion of small seed gold particles (2−5 nm). Gold nanoparticles were formed as indicated by the brown color. In a separate flask, 2 mL of 4 mM silver nitrate (Sigma-Aldrich) was added to 50 mL of Au growth solution (0.2 M CTAB and 1 mM $HAuCl_4$). Then, 0.7 mL of 8 mM L-ascorbic acid (Sigma-Aldrich) solution was added, reducing $HAuCl_4$ to colorless $HAuCl_2$. Subsequent injection of 0.12 mL of seed solution initiated NR growth. The NR growth process was completed within 2 h. NRs were purified by centrifugation twice at 14 000 rpm for 20 min and were redispersed in DI water. The physical dimension of the NRs was characterized by a Hitachi H-7500 transmission electron microscope (TEM) (Hitachi Ltd., Tokyo, Japan), and their hydrodynamic size and surface zeta potential were measured by dynamic light scattering (ZetaSizer NanoZS90, Malvern Instruments, Worcestershire, UK).

Preparation of ScFv EGFR and ATF. The ScFv B10 clone was isolated from the YUAN-FCCC human naive phage display library using solid phase biopanning methods. Large quantities were obtained from lysates of transformed TG1 *Escherichia coli* competent cells (Biochain Institute Inc., Hayward, CA, USA) after Ni^{2+} NTA-agarose column (Qiagen, Valencia, CA, USA) separation. The protein purity was greater than 95%, as determined by using sodium dodecyl sulfate (SDS)-PAGE. For ATF peptide production, a cDNA fragment encoding amino acids 1 to 135 of mouse uPA was isolated by polymerase chain reaction amplification and then cloned into the pET101/D-TOPO expression vector (Invitrogen, Carlsbad, CA, USA). Recombinant ATF peptides were expressed in *Escherichia coli* BL21 (Invitrogen) and purified from bacterial extracts under native conditions using Ni^{2+} NTA-agarose columns.

Au NR PEGylation and Ligand Conjugation. Peptide ligands (ScFv EGFR, ATF, and c(RGDfK) were purchased from Peptide Interactional (Louisville, KY, USA) and were conjugated to Au NRs in a three-step procedure: (i) 50 μL of 1 mM mPEG-SH (MW = 5K, Laysan Bio, Inc., Arab, AL, USA) was added to 10 mL of 1nM Au NRs, and the solution mixture was stirred for 10 min. PEGylated NRs were centrifuged at 14 000 rpm for 10 min and were redispersed in 10 mL of DI water. (ii) A 300 μL amount of 1 mM HOOC-PEG-SH (MW = 5K, Rapp Polymers, Tubingen, German) was added and the solution was stirred for 1 h, resulting in a mixed layer of mPEG-SH and HOOC-PEG-SH on the NR surface. The solution was centrifuged twice at 14 000 rpm for 10 min and was redispersed in 100 μL of MES pH 5.5 buffer. (iii) A 0.2 mg amount of EDC and 0.5 mg of sulfo-NHS (Thermo Scientific, Rockford, IL, USA) were incubated with the functionalized Au NRs for 15 min to activate the carboxyl groups on the Au NRs. Excess EDC/sulfo-NHS was removed by centrifugation at 14 000 rpm for 10 min, and the activated NRs were mixed with the peptide ligands (ScFv EGFR, ATF, or c-RGD) in PBS buffer (pH 7.4) in a NR:ligand molar ratio of 1:1000. The solution was gently shaken for 2 h at RT and then stored at 4 °C. Prior to use, the NR conjugates were centrifuged to separate free reactants. At each step, hydrodynamic size and zeta potential were measured by the ZetaSizer Nano ZS90.

Cell Culture and Au NR Cellular Binding. Human small-cell lung cancer carcinoma A549 cells were cultured in RPMI medium (Mediatech, Inc., Manassas, VA, USA) plus 10% fetal bovine serum (FBS) (Gemini Bio-Products, West Sacramento, CA, USA) at 37 °C under 5% CO_2. For dark-field imaging, the cells were grown on eight-well Lab-Tek chamber slides (Fisher Scientific, Pittsburgh, PA, USA) for 2 days. Then the Au NR conjugates were incubated with cultured cells for 2 h at 37 °C or 1 h at 4 °C. The cells were washed with 1× PBS and fixed with paramaldehyde before dark-field imaging using an Olympus IX70 microscope.

Tumor Inoculation and Au NR Injection. Female nu/nu mice, 7−8 weeks of age, were obtained from Taconic (Hudson, NY, USA). Mice were injected subcutaneously in the flank with 1×10^6 A549 cells suspended in 10 μL PBS. The tumors were allowed to grow for 1−2 weeks to reach a volume of ~100 mm^3. Tumor-bearing mice were administered with Au NR conjugates via tail vein injection.

ICP-MS. Organs and tumors were collected, washed in PBS buffer, and dried at 60 °C for 3 days. The dried tissues were dissolved in concentrated nitric acid (70%, 5 mL for liver and 1 mL for all others, gently shaken for 7 days). Tissue debris was removed by centrifugation at 3000 rpm for 10 min. After dilution in DI water, the gold content was analyzed by ICP-MS (HP 4500, Agilent Technologies, Santa Clara, CA, USA).

Histology and Silver Enhancement. Organs and tumors were collected and fixed in 10% buffered formalin (Sigma-Aldrich). Samples were dehydrated, embedded, and sectioned into 4 μm thick slices. The tissue sections were dewaxed with xylene, washed consecutively with 100%, 90%, 70%, and 30% ethanol, and immersed in a silver enhancement solution, which is composed of equal amounts of solutions A and B from the Silver Enhancer Kit (Sigma-Aldrich). After rinsing, the tissue sections were fixed with 2.5% sodium thiosulfate (Sigma-Aldrich) for 3 min, immersed in hematoxylin (Sigma-Aldrich) for 40 s, washed with DI water, and then mounted for bright-field light imaging.

Transmission Electron Microscopy. Organs and tumors were first fixed in 2.5% glutaraldehyde (in 0.1 M sodium cacodylate, pH 7.4) and then stained by OsO_4 and $K_4Fe(CN)_6$ according to standard procedures. Tissue blocks in Epon resins were sectioned to around 100 nm in thickness for TEM imaging.

Conflict of interest: The authors declare that they have no competing financial interests.

Acknowledgment. This work was supported by grants from the NCI Centers of Cancer Nanotechnology Excellence (CCNE) Program (U54CA119338) and the Specialized Program of Research Excellence (SPORE) in Head and Neck Cancer (P50CA128613). We also thank Gregory Adams at Fox Chase Cancer Center for providing the ScFv B10 plasmid construct, and the Emory Robert P. Apkarian Integrated Electron Microscopy Core for TEM imaging of tissue sections. D.M.S. and S.M.N. are Distinguished Cancer Scholars of the Georgia Cancer Coalition (GCC).

Supporting Information Available: Additional biodistribution data of control and targeted gold nanorods. This material is available free of charge *via* the Internet at http://pubs.acs.org.

REFERENCES AND NOTES

1. Ferrari, M. Cancer Nanotechnology: Opportunities and Challenges. *Nat. Rev. Cancer* **2005**, *5*, 161–171.
2. Farokhzad, O. C; Langer, R. Nanomedicine: Developing Smarter Therapeutic and Diagnostic Modalities. *Adv. Drug Delivery Rev.* **2006**, *58*, 1456–1459.
3. Nie, S.; Xing, Y.; Kim, G. J.; Simons, J. M. Nanotechnology Applications in Cancer. *Annu. Rev. Biomed. Eng.* **2007**, *9*, 257–288.
4. Sanhai, W. R.; Sakamoto, J. H.; Canady, R.; Ferrari, M. Seven Challenges for Nanomedicine. *Nat. Nanotechnol.* **2008**, *3*, 242–244.
5. Heath, J. R; Davis, M. E. Nanotechnology and Cancer. *Annu. Rev. Med.* **2008**, *59*, 251–265.
6. Davis, M. E.; Chen, Z(G).; Shin, D. M. Nanoparticles Therapeutics: An Emerging New Treatment Modality for Cancer. *Nat. Rev. Drug Discovery* **2008**, *7*, 771–782.
7. Cho, K. J.; Wang, X.; Nie, S.; Chen, Z(G).; Shin, D. M. Therapeutic Nanoparticles for Drug Delivery in Cancer. *Clin. Cancer Res.* **2008**, *14*, 1310–1316.
8. Riehemann, K.; Schneider, S. W.; Luger, T. A; Godin, B.; Ferrari, M.; Fuchs, H. Nanomedicine-Challenge and Perspectives. *Angew. Chem., Int. Ed.* **2009**, *48*, 872–897.
9. Philips, M. A.; Gran, M. L.; Peppas, N. A. Targeted Nanodelivery of Drugs and Diagnostics. *Nano Today* **2010**, *5*, 143–159.
10. Nie, S. M. Understanding and Overcoming Major Barriers in Cancer Nanomedicine. *Nanomedicine* **2010**, *5*, 523–528.
11. Jain, R. K. Transport of Molecules, Particles, and Cells in Solid Tumors. *Annu. Rev. Biomed. Eng.* **1999**, *1*, 241–63.
12. Maeda, H.; Wu, J.; Sawa, T.; Matsumura, Y.; Hori, K. Tumor Vascular Permeability and the EPR Effect in Macromolecular Therapeutics: A Review. *J. Controlled Release* **2000**, *65*, 271–84.
13. Matsumura, Y.; Maeda, H. A New Concept for Macromolecular Therapeutics in Cancer-Chemotherapy−Mechanism of Tumoritropic Accumulation of Proteins and

the Antitumor Agent Smancs. *Cancer Res.* **1986**, *46*, 6387–6392.
14. Pirollo, K. F.; Chang, E. H. Does a Targeting Ligand Influence Nanoparticle Tumor Localization or Uptake. *Trends Biotechnol.* **2008**, *26*, 552–555.
15. Kirpotin, D. B.; Drummond, D. C.; Shao, Y.; Shalaby, M. R.; Hong, K.; Nielsen, U. B.; Marks, J. D.; Benz, C. C.; Park, J. W. Antibody Targeting of Long-Circulating Lipidic Nanoparticles Does Not Increase Tumor Localization But Does Increase Internalization in Animal Models. *Cancer Res.* **2006**, *66*, 6732–6740.
16. Bartlett, D. W.; Su, H.; Hildebrand, I. J.; Weber, W. A.; Davis, M. E. Impact of Tumor-Specific Targeting on the Biodistribution and Efficacy of Sirna Nanoparticles Measured by Multimodality *in Vivo* Imaging. *Proc. Natl. Acad. Sci. U. S. A.* **2007**, *104*, 15549–15554.
17. Choi, C. H. J; Alabi, C. A.; Webster, P.; Davis, M. E. Mechanism of Active Targeting in Solid Tumors with Transferrin-Containing Gold Nanoparticles. *Proc. Natl. Acad. Sci. U. S. A* **2010**, *107*, 1235–1240.
18. Schmidt, M. M.; Wittrup, K. D. A Modeling Analysis of the Effects of Molecular Size and Binding Affinity on Tumor Targeting. *Mol. Cancer Ther.* **2009**, *8*, 2861–2871.
19. Garanger, E.; Boturyn, D.; Dumy, P. Tumor Targeting with RGD Peptide Ligands—Design of New Molecular Conjugates for Imaging and Therapy of Cancers. *Anticancer Agents Med. Chem.* **2007**, *7*, 552–558.
20. de Bruin, K.; Ruthardt, N.; Von Gersdorff, K.; Bausinger, R.; Wagner, E.; Ogris, M.; Bräuchls, C. Cellular Dynamics of EGF Receptor-Targeted Synthetic Viruses. *Mol. Ther.* **2007**, *15*, 1297–1305.
21. Hilgenbrink, A. R.; Low, P. S. Folate Receptor-Mediated Drug Targeting: From Therapeutics to Diagnostics. *J. Pharm. Sci.* **2005**, *94*, 2135–2146.
22. Xu, L.; Pirollo, K. F.; Tang, W. H.; Rait, A.; Chang, E. H. Transferrin-Liposome-Mediated Systemic P53 Gene Therapy in Combination with Radiation Results in Regression of Human Head and Neck Cancer Xenografts. *Hum. Gene Ther.* **1999**, *10*, 2941–2952.
23. Daniels, T. R.; Delgado, T.; Rodriguez, J. A.; Helguera, G.; Penichet, M. L. The Transferrin Receptor Part I: Biology and Targeting with Cytotoxic Antibodies for the Treatment of Cancer. *Clin. Immunol.* **2006**, *121*, 144–158.
24. Dass, C. R.; Choong, P. F. Selective Gene Delivery for Cancer Therapy Using Cationic Liposomes: *In Vivo* Proof of Applicability. *J. Controlled Release* **2006**, *113*, 155–163.
25. Koyama, Y.; Hama, Y.; Urano, Y.; Nguyen, D. M.; Choyke, P. L.; Kobayashi, H. Spectral Fluorescence Molecular Imaging of Lung Metastases Targeting HER2/Neu. *Clin. Cancer Res.* **2007**, *13*, 2936–2945.
26. Fidaroval, E. F.; El-Emir, E.; Boxer, G. M.; Qureshi, U.; Dearling, J. L. L.; Robson, M. P.; Begent, R. H. J.; Trott, K. R.; Pedlley, R. B. Microdistribution of Targeted, Fluorescently Labeled Anti Carcinoembryonic Antigen Antibody in Metastatic Colorectal Cancer: Implications for Radioimmunotherapy. *Clin. Cancer Res.* **2008**, *14*, 2639–2646.
27. Gabizon, A.; Horowitz, A. T.; Goren, D.; Tzemach, D.; Shmeeda, H.; Zalipsky, S. In Vivo Fate of Folate-Targeted Polyethylene-Glycol Liposomes in Tumor-Bearing Mice. *Clin. Cancer Res.* **2003**, *9*, 6551–6559.
28. Montet, X.; Funovics, M.; Montet-Abou, K.; Weissleder, R.; Josephson, L. Multivalent Effects of RGD Peptides Obtained by Nanoparticle Display. *J. Med. Chem.* **2006**, *49*, 6087–6093.
29. McNeeley, K. M.; Annapragada, A.; Bellamkonda, R. V. Decreased Circulation Time Offsets Increased Efficacy of Pegylated Nanocarriers Targeting Folate Receptors of Glioma. *Nanotechnology* **2007**, *18*, 385101.
30. Geng, Y.; Dalhaimer, P.; Cai, S.; Tsai, R.; Tewari, M.; Minko, T.; Discher, D. E. Shape Effects of Filaments Versus Spherical Particles in Flow and Drug Delivery. *Nat. Nanotechnol.* **2007**, *2*, 249–255.
31. Park, J. H.; von Maltzahn, G.; Zhang, L; Derfus, A. M.; Simberg, D.; Harris, T. J.; Ruoslahti, E.; Bhatia, S. N.; Sailor, M. J. Systematic Surface Engineering of Magnetic Nanoworms for *in Vivo* Tumor Targeting. *Small* **2009**, *5*, 694–700.
32. Rosen, A. L.; Hieftje, G. M. Inductively Coupled Plasma Mass Spectrometry and Electrospray Mass Spectrometry for Speciation Analysis: Applications and Instrumentation. *Spectrochim. Acta, Part B* **2004**, *59*, 135–146.
33. Huang, X.; El-Sayed, I. H.; Qian, W.; El-Sayed, M. A. Cancer Cell Imaging and Photothermal Therapy in the Near-Infrared Region by Using Gold Nanorods. *J. Am. Chem. Soc.* **2006**, *128*, 2115–2120.
34. Ding, H.; Yong, K. T.; Roy, I.; Pudavar, H. E.; Law, W. C.; Bergey, E. J.; Prasad, P. N. Gold Nanorods Coated with Multilayer Polyelectrolyte as Contrast Agents for Multimodal Imaging. *J. Phys. Chem. C* **2007**, *111*, 12552–12557.
35. Oldenburg, A. L.; Hansen, M. N.; Ralston, T. S.; Wei, A.; Boppart, S. A. Imaging Gold Nanorods in Excised Human Breast Carcinoma by Spectroscopic Optical Coherence Tomography. *J. Mater. Chem.* **2009**, *19*, 6407–6411.
36. Agarwal, A.; Huang, S. W.; ODonnell, M.; Day, K. C.; Day, M.; Kotov, N.; Ashkenazi, S. Targeted Gold Nanorod Contrast Agent for Prostate Cancer Detection by Photoacoustic Imaging. *J. Appl. Phys.* **2007**, *102*, 064701.
37. Li, P. C.; Wang, C. R. C.; Shieh, D. B.; Wei, C. W.; Liao, C. K.; Poe, C.; Jhan, S.; Ding, A. A.; Wu, Y. N. In Vivo Photoacoustic Molecular Imaging with Simultaneous Multiple Selective Targeting Using Antibody-Conjugated Gold Nanorods. *Opt. Exp.* **2008**, *16*, 18605–18615.
38. Wang, H.; Huff, T. B.; Zweifel, D. A.; He, W.; Low, P. S.; Wei, A.; Cheng, J. X. *In Vitro* and *In Vivo* Two-Photon Luminescence Imaging of Single Gold Nanorods. *Proc. Natl. Acad. Sci. U. S. A.* **2005**, *102*, 15752–15756.
39. Durr, N. J.; Larson, T.; Smith, D. K.; Korgel, B. A.; Sokolov, K; Ben-Yakar, A. Two-Photon Luminescence Imaging of Cancer Cells Using Molecularly Targeted Gold Nanorods. *Nano Lett.* **2007**, *7*, 941–945.
40. Yu, C.; Irudayaraj, J. Quantitative Evaluation of Sensitivity and Selectivity of Multiplex Nanospr Biosensor Arrays. *Biophys. J.* **2007**, *93*, 3684–3692.
41. Wang, C.; Chen, Y.; Wang, T.; Ma, Z.; Su, Z. Biorecognition-Driven Self-Assembly of Gold Nanorods: A Rapid and Sensitive Approach toward Antibody Sensing. *Chem. Mater.* **2007**, *19*, 5809–5811.
42. Mayer, K. M.; Lee, S.; Liao, H.; Rostro, B. C.; Fuentes, A.; Scully, P. T.; Nehl, C. L.; Hafner, J. H. A Label-Free Immunoassay Based upon Localized Surface Plasmon Resonance of Gold Nanorods. *ACS Nano* **2008**, *2*, 687–692.
43. Huang, X.; El-Sayed, I. H.; Qian, W.; El-Sayed, M. A. Cancer Cells Assemble and Align Gold Nanorods Conjugated to Antibodies to Produce Highly Enhanced, Sharp and Polarized Surface Raman Spectra: A Potential Cancer Diagnostic Marker. *Nano Lett.* **2007**, *7*, 1591–1597.
44. von Maltzahn, G.; Park, J. H.; Agrawal, A.; Bandaru, N. K.; Das, S. K.; Sailor, M. J.; Bhatia, S. N. Computationally Guided Photothermal Tumor Therapy Using Long-Circulating Gold Nanorod Antennas. *Cancer Res.* **2009**, *69*, 3892–3900.
45. Takahashi, H.; Niidome, T.; Nariai, A.; Niidome, Y.; Yamada, S. Gold Nanorod-Sensitized Cell Death: Microscopic Observation of Single Living Cells Irradiated by Pulsed Near-Infrared Laser Light in the Presence of Gold Nanorods. *Chem. Lett.* **2006**, *35*, 500–501.
46. Tong, L.; Zhao, Y.; Huff, T. B.; Hansen, M. N.; Wei, A.; Cheng, J. X. Gold Nanorods Mediate Tumor Cell Death by Compromising Membrane Integrity. *Adv. Mater.* **2007**, *19*, 3136–3141.
47. Dickerson, E. B.; Dreaden, E. C.; Huang, X.; El-Sayed, I. H.; Chu, H.; Pushpanketh, S.; McDonald, J. F.; El-Sayed, M. A. Gold Nanorod Assisted Near-Infrared Plasmonic Photothermal Therapy (PPTT) of Squamous Cell Carcinoma in Mice. *Cancer Lett.* **2008**, *269*, 57–66.
48. Li, J. L.; Day, D.; Gu, M. Ultra-Low Energy Threshold for Cancer Photothermal Therapy Using Transferrin-

Conjugated Gold Nanorods. *Adv. Mater.* **2008**, *20*, 3866–3871.
49. Niidome, T.; Akiyama, Y.; Yamagata, M.; Kawano, T.; Mori, T.; Niidome, Y.; Katayama, Y. Poly(ethylene glycol)-Modified Gold Nanorods as a Photothermal Nanodevice for Hyperthermia. *J. Biomater. Sci.* **2009**, *20*, 1203–1215.
50. Jiang, T.; Zhang, C.; Zheng, X.; Xu, X.; Xie, X.; Liu, H.; Liu, S. Noninvasively Characterizing the Different $a_v\beta_3$ Expression Patterns in Lung Cancers with RGD-USPIO Using a Clinical 3.0T MR Scanner. *Int. J. Nanomed.* **2009**, *4*, 241–149.
51. Zhang, C.; Lv, F.; Zhou, L.; Li, X.; Wu, X. X.; Hoffman, R. M. Effect of Verapamil on the Expression of EGFR and NM23 in A549 Human Lung Cancer Cells. *Anticancer Res.* **2009**, *29*, 27–32.
52. Kim, I. Y.; Kang, Y. S.; Lee, D. S.; Park, H. J.; Choi, E. K.; Oh, Y. K.; Son, H. J.; Kim, J. S. Antitumor Activity of EGFR Targeted pH-Sensitive Immunoliposomes Encapsulating Gemcitabine in A549 Xenograft Nude Mice. *J. Controlled Release* **2009**, *140*, 55–60.
53. Yamamoto, M.; Ikeda, K.; Ohshima, K.; Tsugu, H.; Kimura, H.; Tomonaga, M. Increased Expression of Low Density Lipoprotein Receptor-related Protein/a2-Macroglobulin Receptor in Human Malignant Astrocytomas. *Cancer Res.* **1997**, *57*, 2799–2805.
54. Hattori, N.; Sisson, T. H.; Xu, Y.; Desai, T. J.; Simon, R. H. Participation of Urokinase-Type Plasminogen Activator Receptor in the Clearance of Fibrin from the Lung. *Am. J. Physiol. Lung Cell Mol. Physiol.* **1999**, *277*, 573–579.
55. Hood, J. D.; Cheresh, D. A. Role of Integrin in Cell Invasion and Migration. *Nat. Rev. Cancer* **2002**, *2*, 91–100.
56. Jin, H.; Varner, J. Integrins: Roles in Cancer Development and as Treatment Targets. *Br. J. Cancer* **2004**, *90*, 561–565.
57. Blasi, F.; Carmeliet, P. uPAR: a Versatile Signaling Orchestrator. *Nat. Rev. Mol. Biol.* **2002**, *3*, 933–943.
58. Nikoobakht, B.; El-Sayed, M. A. Preparation and Growth Mechanism of Gold Nanorods (NRs) Using Seed-Mediated Growth Method. *Chem. Mater.* **2003**, *15*, 1957–1961.
59. Josephson, L.; Tung, C. H.; Moore, A.; Weissleder, R. High-Efficiency Intracellular Magnetic Labeling with Novel Superparamagnetic-Tat Peptide Conjugates. *Bioconjugate Chem.* **1999**, *10*, 186–191.
60. Gao, X.; Cui, Y.; Levenson, R. M.; Chung, L. W. K.; Nie, S. In Vivo Cancer Targeting and Imaging with Semiconductor Quantum Dots. *Nat. Biotechnol.* **2004**, *22*, 969–976.
61. Gu, F.; Zhang, L.; Teply, B. A.; Mann, N.; Wang, A.; Radovic-Moreno, A. F.; Langer, R.; Farokhzad, O. C. Precise Engineering of Targeted Nanoparticles by Using Self-Assembled Biointegrated Block Copolymers. *Proc. Natl. Acad. Sci. U. S. A.* **2008**, *105*, 2586–2591.